Study of the interfacial reactions controlling the spreading of Al on Ni

Youqing Sun[a,*], Ensieh Yousefi[a], Anil Kunwar[b,a], Nele Moelans[a], David Seveno[a], Muxing Guo[a],

[a]*Department of Materials Engineering, KU Leuven, Kasteelpark Arenberg 44, 3001 Leuven, Belgium*

[b]*Faculty of Mechanical Engineering, Silesian University of Technology, Konarskiego 18A, 44-100 Gliwice, Poland*

Corresponding author. *Email address: youqing.sun@kuleuven.be (Y. Sun).*

Abstract

Despite the importance in high-temperature processing, wettability studies focusing on liquid aluminum (Al) on solid nickel (Ni) at high temperatures are scarce due to the difficulty of performing experiments and the complexity of interfacial physical and chemical activities. The effects of interrelated multi-factors, including intermetallic compounds (IMCs) formation and diffusion on wetting dynamics is still debatable. Therefore, in this study, we investigated the reactive spreading of liquid Al on solid Ni by using the combined pendant/sessile drop method between 750 and 950°C. The effects of Ni dissolution into Al on the spreading dynamics were limited due to the low Ni solubility below 950°C. Two continuous Al-rich IMC layers, Al_3Ni and Al_3Ni_2 layers formed at the Al/Ni interface during the isothermal holding stage and affect the final wetting behavior. Additional capillary quenching experiments confirmed that the Al_3Ni phase was the first formed phase. At equilibrium, the Al_3Ni layer was pinned at the triple-phase line at 750°C while it can spread ahead of the liquid front at higher temperatures. This process may be the main reason why at higher temperatures a better spreading is observed as the Al_3Ni layer has a larger affinity to Al than the pure Ni substrate.

Keywords: liquid metal; solid metal; reactive wetting; interfacial reactions

1. Introduction

The presence of Liquid Al in contact with solid Ni is commonly encountered in high-temperature processes, such as casting [1], brazing [2], coating [3] welding [4] and fabricating Al/Ni composite materials [5, 6]. For these processes, the properties of the final products are closely related to the wettability between liquid Al and solid Ni at high temperatures. Thus understanding how solid Ni is wetted by liquid Al has a practical significance and should help to better control these high-temperature processes. However, wettability studies of liquid

Al/solid Ni systems are very scarce due to both the difficulty in performing wetting experiments at high temperatures in a well-controlled environment [7] and the complexity of the interfacial reactions associated with the spreading process. Liquid Al/solid Ni systems are highly reactive, Al can react with Ni over a large temperature range (e.g., 400-1600^{o} C) and forms multiple intermetallic compounds (IMCs) [8]. The interfacial reactions lead to significant changes in the surface and interface morphology and chemistry, thus affecting wettability. Therefore, apart from considering the effects of inertial, viscous, and capillary forces, studies focusing on the wettability of liquid Al on solid Ni substrate also requires to include interfacial reactions into the classical wetting dynamics theories [9].

Several well-developed spreading models incorporating reactive wetting have been proposed. Aksay et al. [10] analyzed the wettability between liquid Ag and solid SiC, and proposed that the free energy associated with the reactions contributes mainly to enhance the wetting driving force. The main difficulty lies in the calculation of the Gibbs free energy since it varies during the wetting process. Eustathopoulos et al. [11] studied the wettability between a liquid CuSi alloy and solid vitreous carbon (C_v), concluding that the equilibrium contact angle was nearly equal to that on the new SiC layer formed at the interface through interfacial reactions between Si and C_v. Based on this observation, they proposed the reaction product control model in which the equilibrium contact angle was determined by the wettability between the liquid phase and the new reaction products (RPs, including carbides, oxides, etc.) instead of that the liquid phase and the parent metal substrate. Moreover, the spreading dynamics, were controlled by interfacial reactions, especially by those taking place at the triple-phase line where the fresh RPs can form and expand together with the spreading liquid. These reactions, in turn, are determined by the diffusion of reacting species in the liquid alloy (e.g. Si in CuSi alloy) to, or from, the triple-phase line and by local reaction kinetics at the triple-phase line (e.g. the SiC formation). Diffusion-controlled wetting [12] and reaction-controlled wetting [13] were then defined based on these respective determining processes. The slower process of these two eventually controls the overall reaction dynamics. In terms of reaction-limited wetting, the relationship between spreading dynamics and the RPs formation at the interface were experimentally evidenced for NiSi/C_v systems [14], pure Si on Si_3Ni4 [15], Ti-containing Ni based alloys on AlN [16]. Diffusion-limited wetting was proposed by Mortensen et al. [12], in which the spreading velocity varied linearly with dynamic contact angles. They found that this model agrees well with Ti containing Cu based alloys on C_v [17]. The alloying element Ti could diffuse to the triple-phase line and react with the solid, resulting in the formation of TiC at the

interface, then improving wettability significantly.

However, all models mentioned above are mainly developed based on liquid metal/solid ceramic systems. For liquid metal/solid metal systems, the dissolution and reactions at interfaces are usually more intense and rapid due to the fact that they have similar lattice constant and a larger affinity to each other. Whether models mentioned above can still work well for metallic systems is still largely unknown. Additionally, the rapid diffusion from the interface may significantly change the surface tension of the pure liquid metal, complicating even further the spreading dynamics. Recently, researchers started to pay more attention to liquid metal/solid metal systems, such as Sn/Cu [18], Sn/Al [19], Al 4043/steel [20], or Al 4043/Ti [21]. The common point of these studies is that the substrate surfaces are initially covered by an oxide film, and interfacial reactions can remove the oxide layer, thus improving wetting. However, discussions about the IMCs formation stage (i.e. cooling or isothermal holding period) and their formation sequence when multiple phases formed at the interface are also neglected, even though only primary phases forming during the isothermal holding stage could affect wettability.

In this study, we investigated the reactive spreading of liquid Al on solid Ni by using a combined pendant/sessile drop method under ultra-high vacuum (UHV) at 750-950°C. The interfacial structures and the primary phase that affect wettability were identified by additional capillary quenching experiments. The correlations between the spreading dynamics, equilibrium state of the Al/Ni systems and interfacial interactions were also analysed. The main objective of this study is to provide an in-depth understanding of reactive wetting in liquid metal/solid metal systems and, especially, of the role of IMC-formation in the wetting dynamics. This study provides a novel view on reactive wetting and new insights important for the guidance of high temperature processing techniques.

2. Experimental methods

2.1. Materials

The materials used in wetting experiments were high-purity (>99.95%) Ni and electrolytic Al (>99.95%). The dimensions of the cylindrical Ni substrates were 16 mm in diameter, and 5 mm in thickness. Before the wetting experiments, the surfaces of Ni substrates were polished and cleaned ultrasonically.

2.2. Surface tension and spreading dynamics

The wetting experiments were performed in an advanced experimental system using the

combined pendant/sessile drop method as detailed by Sobczak et al. [22] and is illustrated in Figure 1. In this specialized equipment, the substrate and the metal are heated separately (non-contact heating), and the oxidized layer (if any) on the liquid metal surface is removed by squeezing it out against the Al_2O_3 injector outlet of diameter 3 mm. The injector sets together with Ni substrates were preferentially placed in a small load-lock cold chamber (10^{-4} Pa) and preheated at 423 K for 15 min to remove absorbed gases. Then they were transferred to the operational UHV chamber (turbomolecular pumpset DN40KF) for the test. The oxygen partial pressures are 1.15×10^{-7}, 9.19×10^{-9} and 7.09×10^{-9} Pa at 750, 850 and 850°C, respectively. This pressure value is low enough when compared to values conducted for Al/Ni reaction experiments [23, 24] or Al surface tension measurement [25]. The whole experimental process was imaged (1000 frames·s^{-1}) using a digital camera (Microtron 310) with an additional LED backlight. When the furnace reached the desired temperature (750, 850 and 950 °C), the droplet was squeezed out, then contacted the Ni substrate and spreads. The isothermal holding stage from the moment the droplet started to be squeezed out to the end was 900s. The specimens (substrates and droplets) were then rapidly moved to the cold chamber and naturally cooled down.

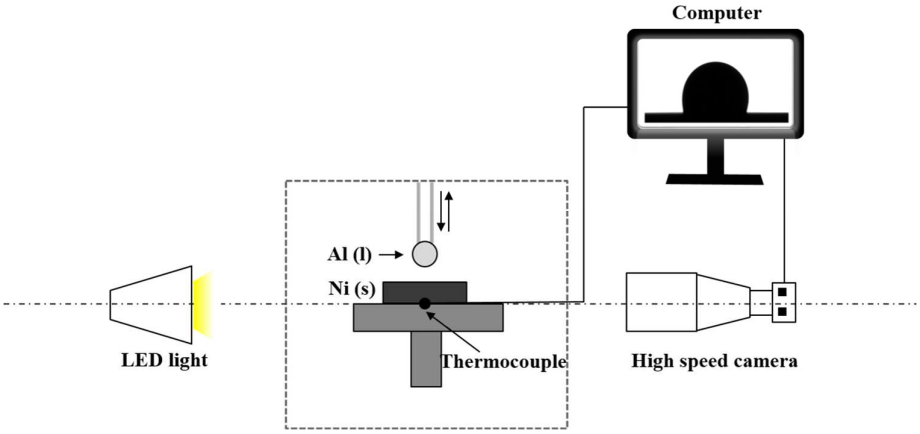

Figure 1 *Schematic of the experimental setup. Wetting experiment.*

Figure 2 illustrates the wetting process of liquid Al on Ni substrate used in the current study. A stable Al pendant drop was firstly squeezed out from the Al_2O_3 injector at the desired temperature (Figure 2a), from which the liquid surface tension could be determined by first detecting the liquid/vapor interface on the collected images (2000-4000 images per experiment) [26] and then adjusting a solution of the Laplace-Young equation (SCA20 software from Dataphysics [27]) to the droplet shape. The Worthington (W_O) number described as Equation 1 was calculated to characterize the accuracy of the measurement:

$$W_O = \frac{\Delta \rho g V}{\pi \sigma_{lv} D_t} \quad (1)$$

where $\Delta\rho$ is the difference between the density of the liquid phase and that of the surrounded atmosphere. Since the UHV chamber was used in the present experiment, $\Delta\rho$ can be considered to be equal to the density of liquid Al (ρ). g is the gravitational acceleration (9.81 m/s^2). V is the volume of droplet. σ_{lv} is the measured liquid/vapor surface tension. D_t is the diameter of the injector outlet. In general, if the value of W_O number is close to 1, the measured surface tension is more accurate. In this work, we considered surface tension values when $0.95 \leq W_O \leq 1.05$.

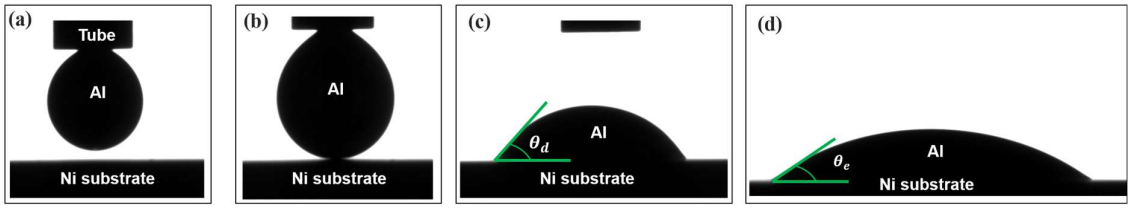

Figure 2 *Illustration of the experimental procedure. (a) pendant drop for surface tension measurement, (b) and (c) spreading dynamics, (d) equilibrium state.*

The time when the droplet contacted the Ni substrate was regarded as the initial moment of the spreading dynamics (Figure 2b). The relaxations of the dynamic contact angle (CA, θ_d) and the contact radius (CR) were extracted from the collected pictures (~20.000 images per experiment) by using the ellipse fitting method in SCA20 software to characterize the spreading process (Figure 2c). When the CA reached equilibrium (Figure 2d, θ_e), the sample was cooled down and cut in the direction perpendicular to the optical axis and prepared for the subsequent microstructure analysis.

2.3. Capillary quenching experiment

The capillary quenching experiments were conducted at 750°C to better characterize the interfacial reactions between liquid Al and solid Ni. Figure 3 shows the experimental set-up. 100 g of electrolytic Al was filled in an alumina crucible which was then charged inside a THERM-AIX vertical furnace (with $MoSi_2$ heating elements). The Al was melted under Ar atmosphere which was purified by passing over Magnesium (Mg) clips. The oxygen content inside the chamber was monitored by a solid state ceramic sensor (Rapidox 2100), yielding an extra low oxygen pressure value at $4.1 \sim 6.6 \times 10^{-12}$ ppm. A piece of Ni cube (5 mm in length) was placed in a special quartz glass capillary with a tapered end (Figure 3a). The capillary together with the Ni cube was quickly introduced into liquid Al. A small volume of liquid Al

was then sucked up and came into contact and then reacted with solid Ni (Figure 3b). After a given reaction time for 1s, 10s, 40s, the capillary was quickly taken out from the liquid, and finally quenched in cooling water. The upper part of the sample (Figure 3c), including the Al/Ni interface is then cut along the longitudinal axis and prepared for microstructure analysis.

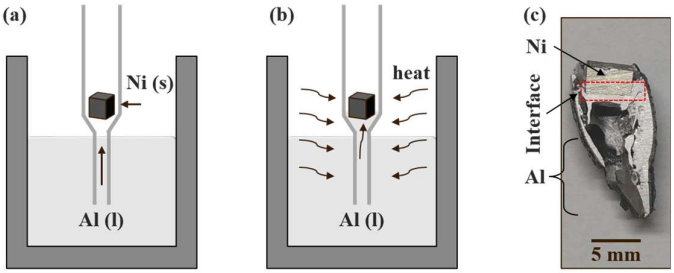

Figure 3 *Schematic of the experimental setup. Capillary quenching experiments. (a) the capillary set was inserted into liquid Al, (b) Al was sucked up to react with Ni, and (c) the upper part of the sample showed the Al/Ni interface.*

2.4. Sample characterization

Samples from both wetting and capillary quenching experiments were firstly mounted in epoxy resin, then grounded by silicon carbide papers and polished with diamond paste. Phase morphologies and microstructure of these samples were analyzed using a high resolution scanning electron microscope (SEM XL-30 LaB_6) equipped with an energy dispersive spectrometer (EDS) detector. The acceleration voltage used to obtain back-scattered electron (BSE) images and elemental analysis was fixed at 20 kV.

3. Experimental results and discussion

3.1. Spreading dynamics

Figure 4 shows how the CAs and CRs varied with time. From Figure 4a and 4b, it can be seen that the wettability improved significantly when temperature increased from 750 to 850°C with θ_e = 32.6° ± 0.15° and 6.7°± 0.03° (Figure 4a, insert) and CR = 5.4 ± 0.03 mm and 7.0 ± 0.05 mm, respectively. The wettability at 850°C is equivalent to that at 950°C as the slight differences of both CAs and CRs are within the error bars. At 750°C, the droplet detached from the capillary at 780 ms and then started oscillating periodically (Figure 4c and Figure 5). The oscillations were clearly visible until 1795 ms, and then started to damp out. The Al droplets eventually spread monotonously on the substrate after 1953 ms. The spreading velocity increased with temperature, as shown in Figure 4d and the insert picture.

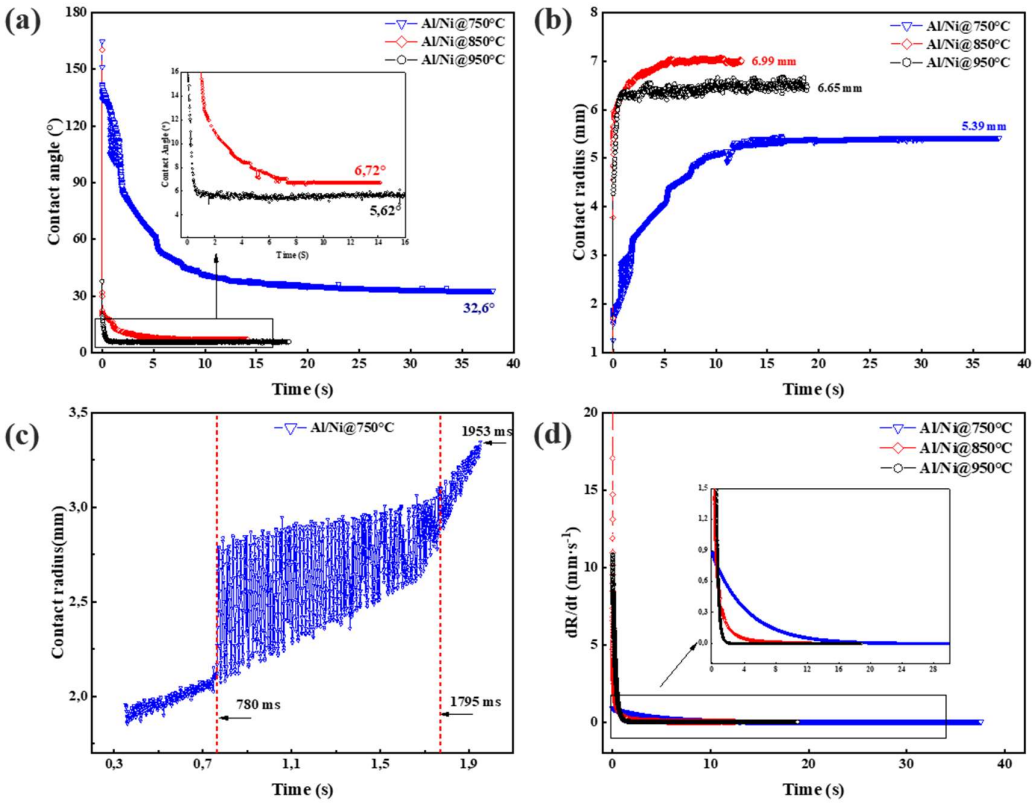

Figure 4 *(a) CAs, and (b) CRs dynamics, (c) the relaxation of the CRs shows oscillation in detail, and (d) spreading velocity of molten Al on solid Ni at 750, 850, and 950°C.*

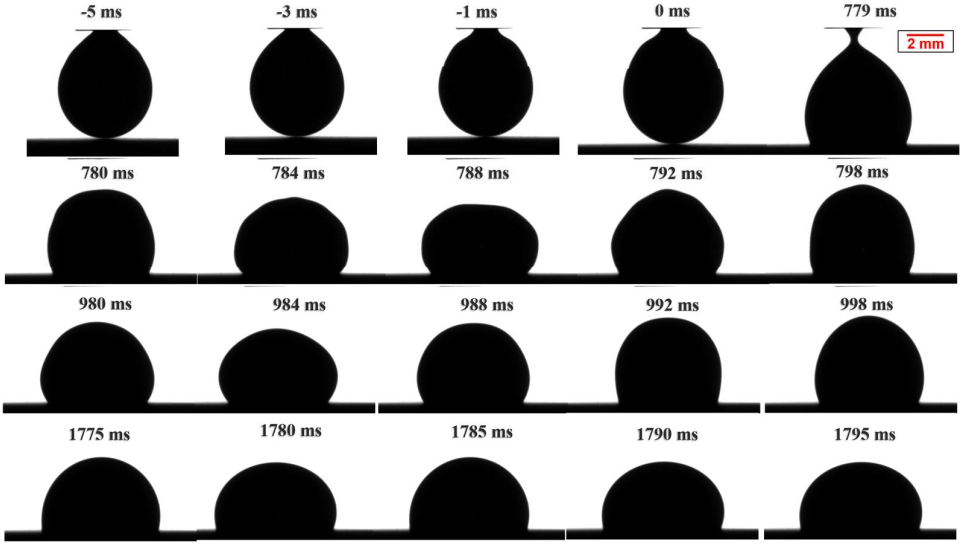

Figure 5 *Time resolved profiles of the droplet during the initial spreading stage at 750°C (Oscillation stage).*

3.2. Surface tension

The Al surface tension values obtained by analyzing the pendant drop in UHV before the liquid Al contacted with Ni are shown in Figure 6. Densities are 2439.4, 2318.4 and 2287.2 $kg \cdot m^{-3}$

at 750, 850 and 950°C respectively [28]. The surface tension and its temperature dependence are described by Equation 2.

$$\sigma_{lv} = 921.39 - 0.2 \times (T - 933) mN \cdot m^{-1} \quad (2)$$

As shown in Figure 6, our results are in good agreement with the measured data from literatures [25, 29, 30]. The deviations may be caused by differences in experimental conditions. The aluminum has a high sensitivity to oxygen in the atmosphere, and it is very difficult to control the oxygen partial pressure precisely during high temperature experiments [31].

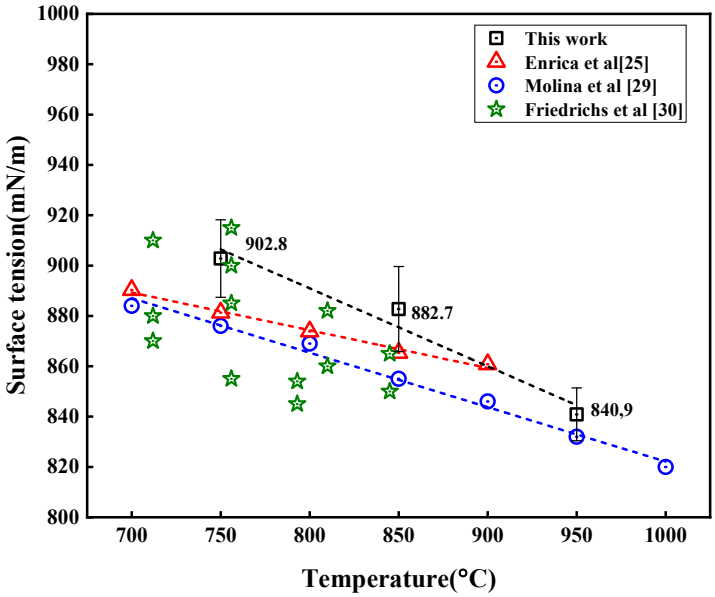

Figure 6 *Surface tension values of pure aluminum in our work and past studies*

At the initial spreading stage, the dynamics are mainly affected by inertial capillary, and viscous forces before reaction and dissolution become dominant [32]. The oscillation during spreading is a typical characteristic for capillary driven liquid. The Ohnesorge number (Oh) and the Weber number (We) are usually used to characterize the dominance of different forces as described in Equation 3 and 4 [33]:

$$\mathrm{Oh} = \frac{\mu}{\sqrt{\rho \sigma_{lv} D_0}} \quad (3)$$

$$\mathrm{We} = \frac{\rho D_0 U_0^2}{\sigma_{lv}} \quad (4)$$

where D_0 is the droplet diameter before contact with the solid surface, and was measured as 4.98 mm from Figure 5 (-5, -3, -1 ms). The method to obtain D_0 is detailed in the Figure S1 in the supplementary material (SM). U_0 is the initial velocity of the spreading liquid at the contact moment (0.9 mm/s at 750°C as shown in Figure 4d) and μ the dynamic viscosity of spreading liquid. At the initial spreading stage, the spreading liquid was considered as pure Al.

The liquid Al viscosity is 1.13 mPa·s at 750°C [34]. Consequently, the Oh and We number are calculated to be 3.4×10^{-4} and 1.1×10^{-5}. According to the work of Schiaffino et al. [35], the liquid conforms to be an inviscid liquid driven by capillary force when the Oh number is far below 10^{-2}~10^{-1}, and the We number is much smaller than 1. Moreover, the oscillation period (τ_{osc}), which is also equal to the reciprocal of the oscillation frequency (f_{osc}), has a relationship with surface tension described by Equation 5 [33]:

$$\tau_{osc} = 1/f_{osc} \approx \sqrt{\rho D_0^3/\sigma_{lv}} \quad (5)$$

The oscillation amplitude around the average value at every point was calculated in Figure 7a. The method to get the average values was detailed in the SM (Figure S2). Based on Figure 7a, the frequency-domain signals which compose the oscillation amplitude were obtained by performing Fast Fourier transform (FFT), as shown in Figure 7b. The description about FFT is detailed in SM. The signal frequency limitation is 1000 Hz, that equals to the sampling frequency of the high speed camera. From Figure 7b, the oscillations are mainly composed by signals with a frequency of 53.59 Hz (after we enveloped the signal magnitude peaks) and the corresponding period is 0.0187s. According to Equation 5, the surface tension value extracted from the oscillation period is 928.21 mN/m, which agrees well with the surface tension value obtained by the present pendant drop method (see Figure 6). This indicates that the capillary force indeed dominates the initial spreading stage at 750°C, which drives the droplet to a dome shape with a constant curvature during spreading [36]. According to Daniel et al. [32], the oscillation disappeared afterwards due to the dissolution and interfacial reactions during spreading. The droplets can reach equilibrium quickly without any visible oscillation at 850 and 950°C (see Figure 4a and b). This phenomenon may also result from the different reaction and interfacial structures at different temperatures and it will be discussed in the Section 3 and 4.

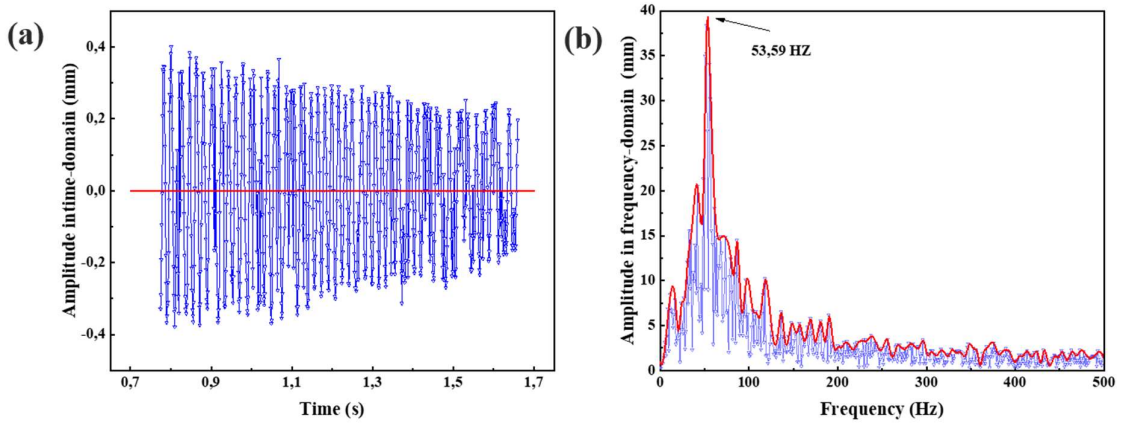

Figure 7 *Contact radius oscillations in the time and frequency domains 750°C. (a) Time domain, (b)*

Frequency domain. The nominal frequency is 53.59 Hz.

After this initial stage, Ni diffusion into liquid Al should both increase liquid surface tension and interface tension (σ_{sl}), therefore affecting spreading. The saturated concentrations of Ni in liquid Al are 7.5, 13 and 18 at% at 750, 850 and 950 °C, respectively [37]. It means that Al/Ni system is a dissolutive system. Generally, the dissolution of the higher melting temperature metal (substrate material) into low melting point liquid increases the surface tension and interface tension at the same time for a binary metal system (except for Au/Si system) [38]. However, our system is not a simple dissolutive system, but combines dissolution and IMCs formation. Figure 8a shows the surface tension of Al-Ni alloys with various Ni contents as a function of temperature. The surface tension dependence on Ni composition at fixed 1400 °C is also shown in Figure 8b. From Figure 8a, the temperature dependence of low Ni content alloys is similar to that of pure Al, suggesting a limited effect of dissolved Ni elements at low Ni concentrations. However, the temperature dependence varies significantly for the alloys with high Ni concentrations (i.e., Ni = 18, 23.5 and 25 at%) when temperatures are higher than 950°C. This is further confirmed in Figure 8b, where the surface tension slightly increases with Ni concentration until 18 at%, the Ni solubility limit at 950°C, beyond that it increases dramatically.

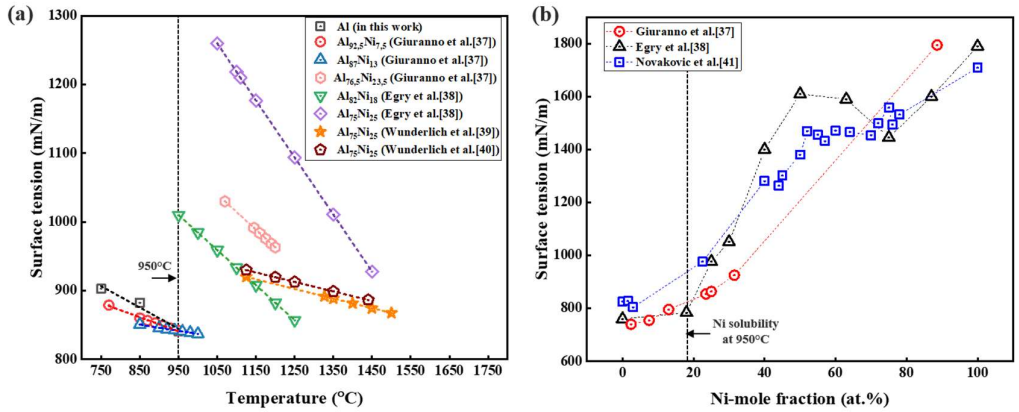

Figure 8 *Surface tension of Al-Ni alloys. (a) surface tension versus temperature, (b) surface tension versus Ni-mole fraction at 1400°C. [39-43]*

The effects of dissolved Ni element on spreading dynamics and wettability are limited in our system. On one hand, the solubility is not large enough to influence surface and interface tension below and at 950°C. On the other hand, the high melting point Ni will increase both surface and interface tension, and then deteriorate wettability. In our system, the wettability improved with higher dissolved Ni amount at higher temperature. Therefore, the dissolution of Ni into the droplet is not considered to pay an important role. The effects of IMCs formation

on the spreading dynamics and wettability are discussed below.

3.3. Formation and growth rate of the intermetallic compounds

Figure 9 shows the microstructure of the Al/Ni interface for understanding interfacial reactions that took place in the wetting experiment. The CRs and CAs of droplets after solidification were measured and compared to the final values obtained at the end of the spreading dynamics (Figure 4a and b). For the sample at 750°C (Figure 9a), both the solidified CAs and CRs are identical to their respective equilibrated ones of the wetting experiment within the error bars (a slight difference could be due to the droplet's shrinkage after solidification). The CAs measured from both isothermal holding stage and room temperature (after solidification) were all below 4° for the wetting tests at 850 and 950 °C (Figure 9b and c), indicating that the Ni substrate was almost completely wetted by liquid Al at high temperatures. The crack in Figure 9b is most likely formed during cooling, caused by the different linear expansion coefficients of the liquid droplet and IMCs layers [38]. No cracks or gaps were detected on the pictures showing droplets at equilibrium (Figure S3 in SM), they could then establish intimate contacts with the substrates during the isothermal heating stage and cracks are produced during the cooling stage. The liquid and solidified Al drops share identical shapes suggesting that spreading mainly occurred during the isothermal holding stage without noticeable influence of the cooling process. Additionally, continuous IMC layers were observed at interfaces under different temperatures.

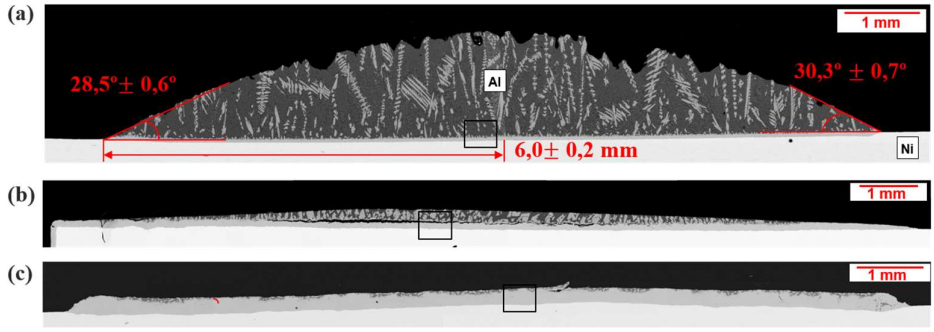

Figure 9 *SEM cross-section pictures of liquid Al /solid Ni systems at (a) 750°C, (b) 850°C, and (c) 950°C. The black rectangles indicate the zones analyzed by EDS and shown in Figure 10.*

Figure 10 shows the results of the EDS analysis on the areas indicated by the black rectangles in Figure 9. Two continuous IMC layers can be found at each interface (Figure 10a-c). A homogenous and thick layer (point #3) is located next to the Ni substrate and on top of this thick layer an irregular and faceted layer (point #2) forms. Some big solid particles (point #1)

were also precipitated in Al drops. The compositions analysis of points #1, 2, and 3 with EDS identifies that the homogeneous layer is Al_3Ni_2 while the faceted layer and big particles within Al droplet is Al_3Ni (Table 1). In addition, Ni was detected in the liquid Al, but no Al was found in the solid Ni substrate (Figure 10d-f). This analysis confirms that there was a significant diffusion of Ni into Al during spreading, whereas the diffusion of Al into Ni substrate was below the detectable limit.

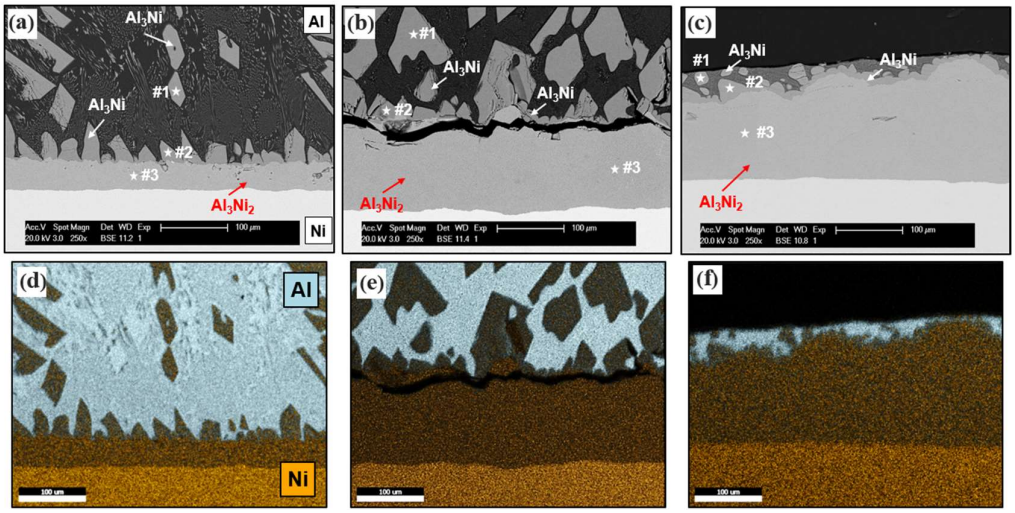

Figure 10 *Magnified SEM pictures and the corresponding elemental mapping images obtained from the experiments performed at (a) (d) 750°C, (b) (e) 850°C, and (c) (f) 950°C.*

Table 1 *EDS analysis results of points in Figure 10.*

Al/Ni systems at different temperatures (°C)	Compositions at different points (Al: at%; Ni: at%)			Phases at different points		
	#1	#2	#3	#1	#2	#3
750	75.09; 24.91	75.23; 24.77	60.30; 39.70			
850	75.62; 24.38	75.45; 24.55	62.20; 37.80	Al_3Ni	Al_3Ni	Al_3Ni_2
950	76.94; 23.06	75.92; 24.08	60.20; 39.80			

During the isothermal holding stage, only the primary phase, that was directly in contact with liquid, can affect spreading. However, previous studies did not come to an agreement on the IMCs formation sequence and on the stage of the wetting process where the IMCs form (see Table 2). Lopez et al. [44] concluded that Al_3Ni primarily precipitates from the liquid phase when the Ni concentration reaches its solubility limit. Al_3Ni_2 develops by further diffusion of Ni into Al_3Ni. However, Ding et al. [45] held the opinion that Al_3Ni_2 forms firstly during cooling, and Al_3Ni is produced by peritectic reactions between solid Al_3Ni_2 phase and liquid Al.

Table 2 *Interfacial reactions in different types of liquid Al/solid Ni diffusion experiments.*

Methods	Temperature (°C)	Primary phase		Secondary phase		Reference
		Phase	When	Phase	When	
Ni/Al/Ni	776	Al_3Ni		Al_3Ni_2	During isothermal holding	[8]
Ni/Al/Ni	720					[44]

Hot-dip	800		During			[46]
Hot-dip	767,817,867		isothermal			[47]
Pour-out	450,485,520		holding			[48]
Al/Ni couple	850	Al_3Ni_2	During cooling	Al_3Ni	During cooling	[45]
Hot-dip	700,800,900					[49]

In this study, the phase formation sequence was unraveled by conducting capillary quenching experiments at 750 °C (see Figure 3). With a short holding time of 1s, Al_3Ni forms at the interface (Figure 11a, 1s). After holding for 10s (Figure11b), Al_3Ni_2 phases precipitate at the interfaces between Al_3Ni and Ni substrate. At 40s (Figure 11c), from certain positions of the continuous Al_3Ni layer, it protrudes into liquid Al meanwhile Al_3Ni also precipitates in liquid Al. These observation indeed agrees with Lopez et al. [42] that Al_3Ni forms first when the Ni concentration reaches its solubility limit and Al_3Ni_2 is then produced as a result of further Ni dissolution into liquid Al. In Figure 11a, the Si element was detected in the droplet but not at the interface. It means that the deoxidation of SiO_2 will lead to dissolution of Si into the droplet, but it will not influence the phase formation sequence of our experiments due to its limited presence at the interface.

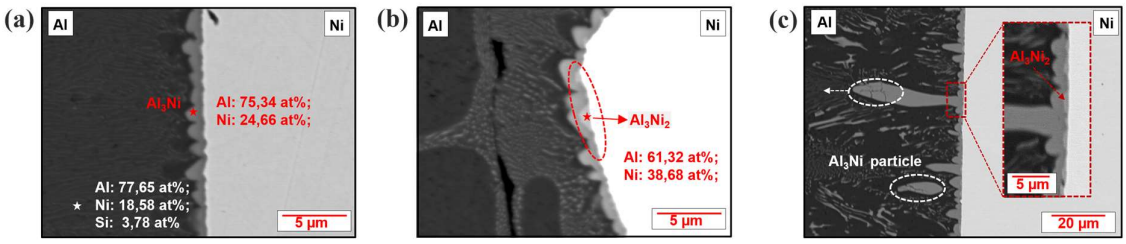

Figure 11 *BSE images of capillary quenching experiments with different holding time at 750 °C. (a) 1s, (b) 10s, and (c) 40s.*

The average thickness of the Al_3Ni_2 layer increases with temperature and mainly contributes to the total IMC thickness (see Figure 10 and 12). On the other hand, the Al_3Ni layer thickness firstly raises from 20.0 to 33.4 µm with temperature increasing from 750 to 850°C, but then decreases to 18.8 µm with temperature further increasing to 950°C (Figure 12). More details about thickness calculation can be found in Figure S4 and Table S1 in the SM.

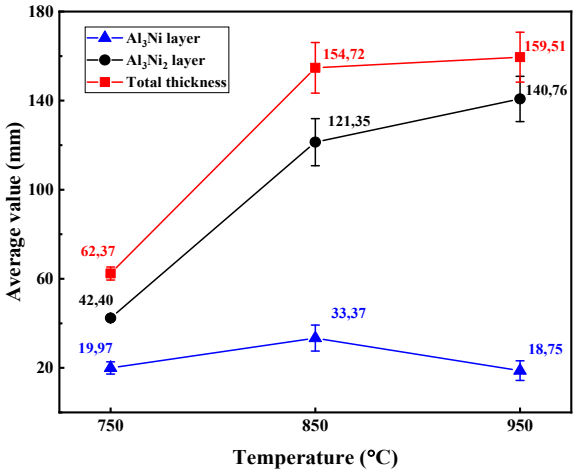

Figure 12 *IMC layer thicknesses.*

The growth constants of the Al_3Ni_2 layer formed and grew in the isothermal holding stage was then studied to compare with those from past studies. It took 6, 5 and 10 s for Al droplets to be squeezed out and contact solid Ni during the isothermal holding stages at 750, 850 and 950°C, respectively. Then time intervals for corresponding interfacial reactions are 894, 895 and 890 s. Compared to these time intervals, the time required for the Al_3Ni_2 formation at the very initial interaction stage can be ignored. Assuming a classical growth model for Al_3Ni_2 as depicted by Equation 6 [50], the growth constants k_1 were calculated and are compared to values obtained in previous studies in Table 2.

$$\Delta x^2 = k_1 t \tag{6}$$

Where Δx is thicknesses of Al_3Ni_2 layer at different temperatures (Figure 12), t is corresponding time interval for interfacial reactions. k_1 is obtained by dividing Δx^2 with t. Figure 13 (specific data is listed in Table S2 in the SM) shows the temperature dependence of the growth constant k_1 expressed by the Arrhenius plot, where the growth constants obtained in this study are in a good agreement with past studies even though their growth constants were obtained at temperatures under the Al melting point. This confirms that the growth of the Al_3Ni_2 layer in our experiments is driven by solid/solid interactions and that the Al_3Ni phase is the primary phase generated from liquid /solid reactions. To be more specific, the solid Ni dissolves into liquid Al and Al_3Ni firstly crystallizes at the Al/Ni interface when the Ni concentration reaches its solubility limit. Then Al_3Ni_2 phase is produced from reactions between Al_3Ni phase and more dissolved Ni from substrates. The growth constants from references [45] and [47] are much larger than those obtained in this current work. This is attributed to the fact that they

calculated the growth constants for the total IMCs layers including both the Al_3Ni_2 and Al_3Ni layers.

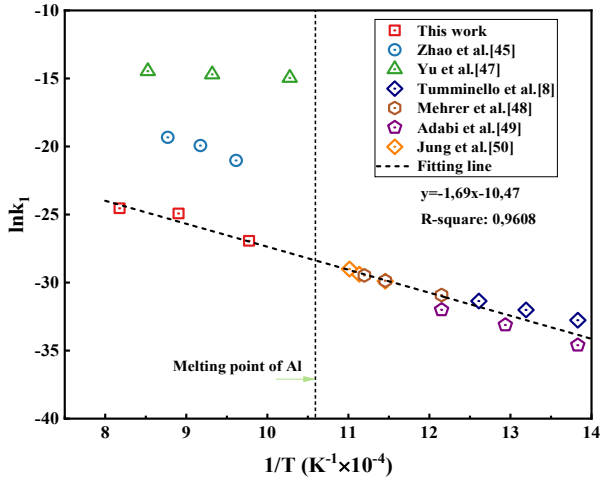

Figure 13 *Growth rate constants versus 1/T. [50-52]*

The Al_3Ni layer thickness decrease for the test at 950°C may due to the fact that it dissolved into liquid Al or transferred into Al_3Ni_2 layer with large reaction rates. Since Al_3Ni is directly in contact with liquid Al during spreading, it should play a major role in the spreading dynamics.

3.4. Effects of the IMCs on the spreading dynamics

Our results show clearly that the IMCs formation play a major beneficial role on spreading. On one hand, the oxygen partial pressure in our experiments is ~10^{-9} Pa. This means that an oxide film may form on the Ni substrate surface since the oxygen film free substrate can only be achieved with oxygen partial pressure less than 10^{-12} Pa [53]. The IMCs formation will then remove the oxide film and produce a fresh surface, therefore improving wettability. On the other hand, the energy of reactions liberated at the interface can increase the driving force of wetting [54]. The spreading dynamics is controlled by the lateral growth of the IMCs in either mechanism mentioned above. In a metastable state, the IMC layer is pinned at the triple-phase line and cannot break through the liquid front due to thermodynamic barriers and reaction kinetics [55]. Alternatively, the IMC layer can extend ahead of the liquid front, overcoming this thermodynamic barrier, to reach an equilibrium state. In this case, the wetting properties are directly determined by the interactions between the liquid and the reaction products if we neglect roughness effects [56]. This was substantiated from the present observation in Figure 14, where the IMC layers were pinned at the triple-phase line at 750 °C (Figure 14a), while

they could extend ahead of the liquid front at 850 and 950°C (Figure 14b). Based on EDS results in Table 3, the Al_3Ni layer firstly extended outward the liquid front and then a large part of it was transferred into the Al_3Ni_2 layer at the interface at high temperatures. By contrast, the Al_3Ni layer was pinned at the liquid front at 750 °C so the subsequently formed Al_3Ni_2 layer cannot extend outward either. The presence of Al atoms ahead of the liquid front is considered to be mainly due to surface diffusion and/or adsorption/desorption mechanism [9], as shown in the upper part of Figure 14b. Since at lower temperature (i.e., 750°C) the activation energy required for adsorption/desorption and/or surface diffusion is larger and the reaction rate is smaller, the Al_3Ni layer can be pinned at the triple-phase line and cannot extend outward the liquid front. No theoretical description of this energy barrier is currently available due to the complexity of the triple-phase zone which should account for the interrelations between interfacial energy, reaction, adsorption, surface diffusion, etc.

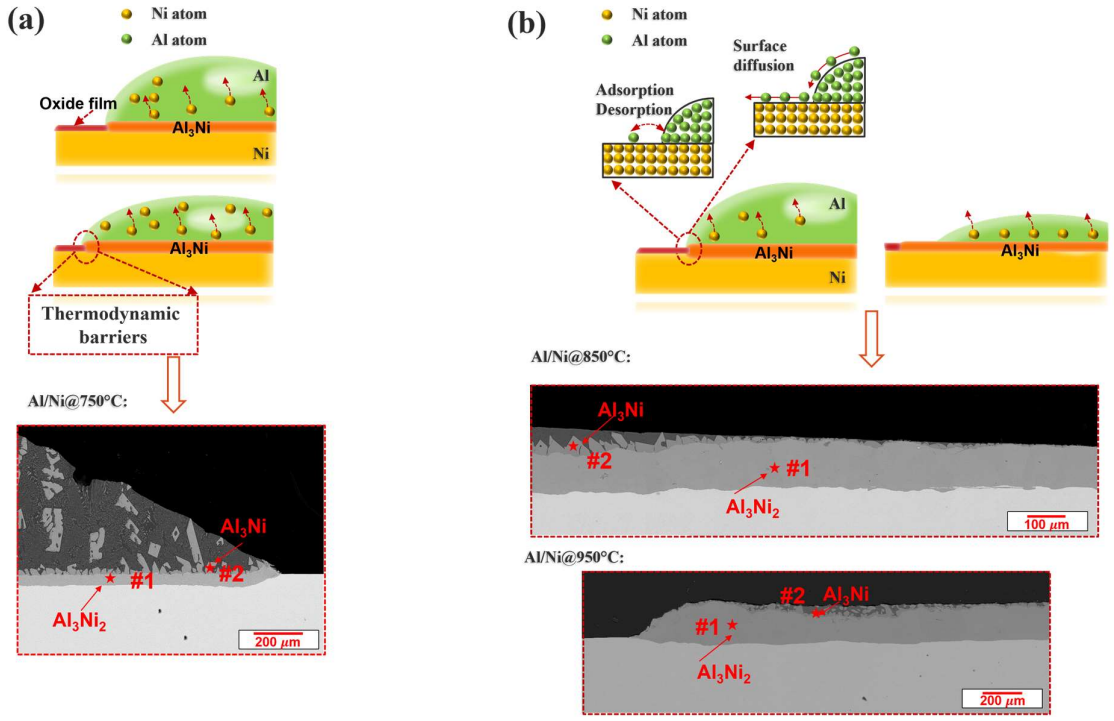

Figure 14 *Schematic views of the triple-phase zones at (a) 750°C, (b) 850 and 950°C and associated SEM pictures*

Table 3 *EDS analysis results of points in Figure 14.*

Al/Ni systems at different temperatures (°C)	Phases at different points (Al: at%; Ni: at%)		Phases at different points	
	#1	#2	#1	#2
750	61.17; 38.83	77.28; 22.72		
850	61.69; 38.31	75.52; 24.28	Al_3Ni_2	Al_3Ni
950	62.66; 37.34	76.72; 23.28		

During the wetting process, the spreading dynamics can be described by a reaction limited

model (Equation 7) as suggested by Dezellus [13]:

$$\ln(\cos\theta_e - \cos\theta_d) = -k_2 t + \ln(\cos\theta_e - \cos\theta_0) \quad (7)$$

where θ_0 represents the initial observable contact angle when Al starts contacting with Ni substrate. k_2 is the spreading kinetic constant. Equation 7 was used to fit the contact angle relaxations as shown in Figure 15a, where the slope of each fitting line is obtained as the corresponding kinetic constant k_2 at each temperature. The kinetic constants were also plotted as a function of $1/T$ (Figure 15b) from which the activation energy (E_a) for reactive wetting was found to be 268.4 kJ/mol. This energy is approximately equal to the sum of the activation energies for the growth of Al_3Ni (136 kJ/mol) [57] and Al_3Ni_2 phases (116±19 kJ/mol) [58], characterizing the influence of interfacial reactions on the spreading dynamics.

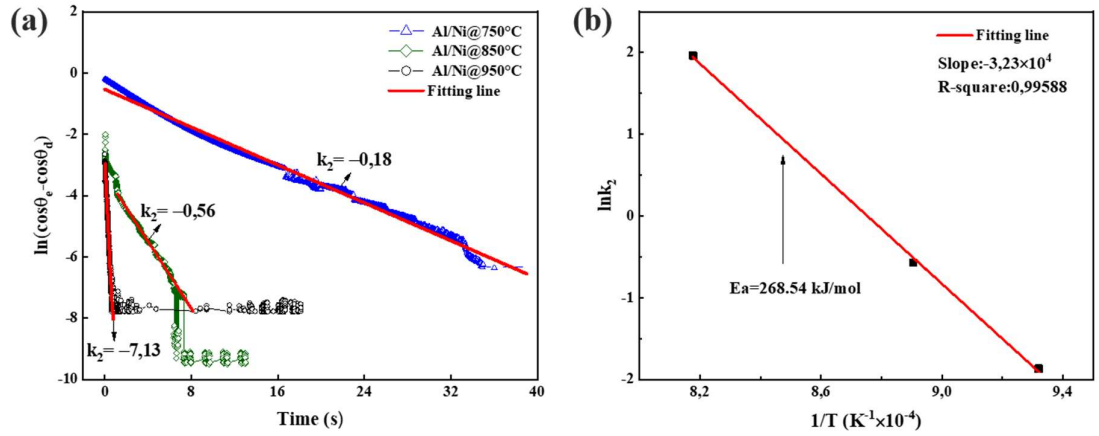

Figure 15 *The spreading dynamics of Al/Ni systems were fitted by reaction-limited model and (a) logarithm of* $\cos\theta_e - \cos\theta_d$ *vs. time, (b) Arrhenius plot of* lnK *against* $1/T$ *for calculation of the spreading activation energy.*

The equilibrium contact angles can be calculated by the Young equation (Equation 8) [59]:

$$\cos\theta_e = \frac{\sigma_{sv} - (\sigma_{sl} + \Delta\sigma_1)}{(\sigma_{lv} + \Delta\sigma_2)} \quad (8)$$

with σ_{sv} is the solid surface tension, $\Delta\sigma_1$ and $\Delta\sigma_2$ are the changes of the σ_{lv} and σ_{sl} due to Ni dissolution. Dividing the numerator and denominator by σ_{lv}, we can get Equation 9:

$$\cos\theta_e = \frac{1}{1 + \Delta\sigma_2/\sigma_{lv}} \left(\frac{\sigma_{sv} - \sigma_{sl}}{\sigma_{lv}} - \frac{\Delta\sigma_1}{\sigma_{lv}} \right) \quad (9)$$

Since $\Delta\sigma_1$ and $\Delta\sigma_2$ can be neglected below and at 950°C, we can finally derive Equation 10:

$$\cos\theta_e = \frac{\sigma_{sv} - \sigma_{sl}}{\sigma_{lv}} = \cos\theta' \quad (10)$$

with θ' the contact angle between liquid Al and different substrates depending on whether the reaction products can move ahead of the liquid front. For equilibrium, at 850 and 950°C, a Al_3Ni phase formed at the Al/Ni interface and can extend ahead of the liquid front, thus θ'

should be equal to the contact angle between the liquid Al and the Al_3Ni layer (θ_1'). Without reaction at the interface, then θ' is equal to the contact angle between liquid Al and solid Ni (θ_2'). At 750°C, the IMC layers cannot move ahead of the triple-phase line, θ' is however supposed to have an intermediate value (θ_3'). In our system, we observed that $\theta_2' > \theta_3' > \theta_1'$. It is indeed plausible since the Al_3Ni layer is more wettable by liquid Al than the pure Ni substrate. Therefore, the equilibrium contact angles at 850 and 950°C are both smaller than that obtained at 750 °C. The wettability at 850°C is equivalent to that at 950°C since they are both controlled by the wettability between liquid Al and the solid Al_3Ni layer.

In conclusion, the spreading dynamics in our experiments agree well with reaction-limited wetting. At equilibrium, the Al_3Ni layer could move outward the triple-phase line at 850 and 950°C but was pinned at 750 °C due to thermodynamic barriers. Consequently wettability is better at high temperatures since the Al_3Ni layer has a larger affinity to Al than the pure Ni substrate.

4. Conclusions

The reactive spreading of liquid Al on solid Ni was investigated by a combined pendant/sessile drop method at 750, 850 and 950°C. The interfacial reactions as well as their correlations with wettability were also studied. The effects of dissolved Ni into Al on the spreading dynamics and wettability were limited due to the low Ni solubility below 950°C. Two continuous IMC layers, Al_3Ni and Al_3Ni_2 layers were formed at the interface during the isothermal holding stage. Al_3Ni first formed at the solid/liquid interface and affected the final wetting properties. The formation of IMCs layer can remove the oxide film on Ni substrate and accelerate spreading. The spreading dynamics agree well with the reaction-limited model, characterizing the influence of the Al_3Ni layer formation. At equilibrium, the Al_3Ni layer was pinned at the triple-phase line at 750°C due to a thermodynamic barrier while it can spread ahead of the liquid front at 850 and 950 °C. Therefore, the wettability is better at high temperatures as the Al_3Ni layer is more wettable than the pure Ni substrate.

Although the present work clarified different configurations at different temperatures (Figure 14), quantitative description of the thermodynamic barrier at the triple-phase line remains unresolved. Moreover, interfacial reactions at the very initial spreading stage (in few milliseconds) should be investigated to comprehensively understand reactive wetting and further improve the reaction-limited model. All these challenges will be explored in future works.

5. CRediT authorship contribution statement

Youqing Sun: Investigation, Writing-original draft, Formal analysis, Data curation, Visualization. **Ensieh Yousefi:** Investigation, Writing – review & editing, Validation. **Anil Kunwar:** Investigation, Writing – review & editing, Validation. **Nele Moelans:** Resources, Supervision, Writing – review & editing, Validation. **David Seveno:** Conceptualization, Resources, Supervision, Writing – review & editing, Validation. **Muxing Guo:** Conceptualization, Resources, Supervision, Writing – review & editing, Validation.

6. Declaration of Competing interest

The authors declare that they have no known competing financial interest or personal relationships that could have appeared to influence the work reported in this paper.

7. Acknowledgement

Youqing Sun thanks the China Scholarship Council (CSC) for financial support (CSC No. 201906370027). The authors would like to thank the research fund of KU Leuven under project C14-17-075.

8. Appendix A

Supplementary material Supplementary data associated with this article can be found at supplementary_material.pdf file.

9. References

[1] C. Suwanpreecha, P. Pandee, U. Patakham, C. Limmaneevichitr, New generation of eutectic Al-Ni casting alloys for elevated temperature services, Materials Science and Engineering: A, 709 (2018) 46-54, https://doi.org/10.1016/j.msea.2017.10.034.

[2] W. Wołczyński, T. Okane, C. Senderowski, D. Zasada, B. Kania, J. Janczak-Rusch, Thermodynamic justification for the Ni/Al/Ni joint formation by a diffusion brazing, International Journal of Thermodynamics, 14 (2011) 97-105, https://doi.org/10.5541/ijot.296.

[3] S. Ip, R. Sridhar, J. Toguri, T. Stephenson, A. Warner, Wettability of nickel coated graphite by aluminum, Materials Science and Engineering: A, 244 (1998) 31-38, https://doi.org/10.1016/S0921-5093(97)00823-X.

[4] H. Wang, L. Liu, F. Liu, The characterization investigation of laser-arc-adhesive hybrid welding of Mg to Al joint using Ni interlayer, Materials & Design, 50 (2013) 463-466, https://doi.org/10.1016/j.matdes.2013.02.085.

[5] G. Min, J.-M. Lee, S.-B. Kang, H.-W. Kim, Evolution of microstructure for multilayered Al/Ni composites by accumulative roll bonding process, Materials Letters, 60 (2006) 3255-3259, https://doi.org/10.1016/j.matlet.2006.03.001.

[6] A. Mozaffari, H.D. Manesh, K. Janghorban, Evaluation of mechanical properties and structure of multilayered Al/Ni composites produced by accumulative roll bonding (ARB) process, Journal of Alloys and Compounds, 489 (2010) 103-109,

https://doi.org/10.1016/j.jallcom.2009.09.022.
[7] N. Sobczak, M. Singh, R. Asthana, High-temperature wettability measurements in metal/ceramic systems–Some methodological issues, Current Opinion in Solid State and Materials Science, 9 (2005) 241-253, https://doi.org/10.1016/j.cossms.2006.07.007.
[8] S. Tumminello, S. Sommadossi, Growth kinetics of intermetallic phases in transient liquid phase bonding process (TLPB) in Al/Ni system, in: Defect and Diffusion Forum, Trans Tech Publ, 2012, pp. 465-470, https://doi.org/10.4028/www.scientific.net/DDF.323-325.465.
[9] D. Seveno, A. Vaillant, R. Rioboo, H. Adao, J. Conti, J. De Coninck, Dynamics of wetting revisited, Langmuir, 25 (2009) 13034-13044, https://doi.org/10.1021/la901125a.
[10] I.A. Aksay, C.E. Hoge, J.A. Pask, Wetting under chemical equilibrium and nonequilibrium conditions, The Journal of Physical Chemistry, 78 (1974) 1178-1183, https://doi.org/10.1021/j100605a009.
[11] N. Eustathopoulos, Dynamics of wetting in reactive metal/ceramic systems, Acta Materialia, 46 (1998) 2319-2327, https://doi.org/10.1016/S1359-6454(98)80013-X.
[12] A. Mortensen, B. Drevet, N. Eustathopoulos, Kinetics of diffusion-limited spreading of sessile drops in reactive wetting, Scripta Materialia, 36 (1997) 645, https://doi.org/10.1016/S1359-6462(96)00431-9.
[13] O. Dezellus, F. Hodaj, N. Eustathopoulos, Progress in modelling of chemical-reaction limited wetting, Journal of the European Ceramic Society, 23 (2003) 2797-2803, https://doi.org/10.1016/S0955-2219(03)00291-7.
[14] V. Bougiouri, R. Voytovych, O. Dezellus, N. Eustathopoulos, Wetting and reactivity in Ni–Si/C system: experiments versus model predictions, Journal of materials science, 42 (2007) 2016-2023, https://doi.org/10.1007/s10853-006-1483-8.
[15] B. Drevet, R. Voytovych, R. Israel, N. Eustathopoulos, Wetting and adhesion of Si on Si3N4 and BN substrates, Journal of the European Ceramic Society, 29 (2009) 2363-2367, https://doi.org/10.1016/j.jeurceramsoc.2009.01.024.
[16] O. Dezellus, N. Eustathopoulos, Fundamental issues of reactive wetting by liquid metals, Journal of Materials Science, 45 (2010) 4256-4264, https://doi.org/10.1007/s10853-009-4128-x.
[17] O. Dezellus, F. Hodaj, A. Mortensen, N. Eustathopoulos, Diffusion-limited reactive wetting: spreading of Cu-Sn-Ti alloys on vitreous carbon, Scripta materialia, 44 (2001) 2543-2549, https://doi.org/10.1016/S1359-6462(01)00946-0.
[18] Q. Lin, F. Li, J. Wang, Wetting of Sn/Cu and Sn/Cu-Sn IMCs at 623–723K, Journal of Alloys and Compounds, 767 (2018) 877-882, https://doi.org/10.1016/j.jallcom.2018.07.201.
[19] Q. Lin, W. Zhong, F. Li, W. Yu, Reactive wetting of tin/steel and tin/aluminum at 350–450° C, Journal of Alloys and Compounds, 716 (2017) 73-80, https://doi.org/10.1016/j.jallcom.2017.05.036.
[20] Q. Lin, P. Jin, R. Cao, J. Chen, Reactive wetting of low carbon steel by Al 4043 and 6061 alloys at 600–750° C, Surface and Coatings Technology, 302 (2016) 166-172, https://doi.org/10.1016/j.surfcoat.2016.06.005.
[21] Q. Lin, F. Li, P. Jin, W. Zhong, Reactive wetting of TA2 pure Ti and TC4 alloy by molten Al 4043 alloy at 873–973 K, Vacuum, 145 (2017) 95-102, https://doi.org/10.1016/j.vacuum.2017.08.034.
[22] N. Sobczak, J. Sobczak, R. Asthana, R. Purgert, The mystery of molten metal, China

537 Foundry, 7 (2010) 425-437.
538 [23] M. Jain, S. Gupta, Formation of intermetallic compounds in the Ni–Al–Si ternary system,
539 Materials characterization, 51 (2003) 243-257, https://doi.org/10.1016/j.matchar.2003.12.002.
540 [24] K. Manukyan, J. Pauls, C. Shuck, S. Rouvimov, A. Mukasyan, K. Nazaretyan, H.
541 Chatilyan, S. Kharatyan, Kinetics and mechanism of ignition in reactive Al/Ni nanostructured
542 materials, The Journal of Physical Chemistry C, 122 (2018) 27082-27092,
543 https://doi.org/10.1021/acs.jpcc.8b09075.
544 [25] J. Molina, R. Voytovych, E. Louis, N. Eustathopoulos, The surface tension of liquid
545 aluminium in high vacuum: the role of surface condition, International journal of adhesion and
546 adhesives, 27 (2007) 394-401, https://doi.org/10.1016/j.ijadhadh.2006.09.006.
547 [26] B. Keene, Review of data for the surface tension of pure metals, International Materials
548 Reviews, 38 (1993) 157-192, https://doi.org/10.1179/imr.1993.38.4.157.
549 [27] D.G. Waugh, J. Lawrence, On the use of CO2 laser induced surface patterns to modify the
550 wettability of poly (methyl methacrylate)(PMMA), Optics and Lasers in Engineering, 48 (2010)
551 707-715, https://doi.org/10.1016/j.optlaseng.2010.01.005.
552 [28] C. Beghi, C. Geel, G. Piatti, Density measurements after tensile and creep tests on pure
553 and slightly oxidised aluminium, Journal of Materials Science, 5 (1970) 331-334,
554 https://doi.org/10.1007/BF02397785.
555 [29] E. Ricci, D. Giuranno, N. Sobczak, Further development of testing procedures for high
556 temperature surface tension measurements, Journal of materials engineering and performance,
557 22 (2013) 3381-3388, https://doi.org/10.1007/s11665-013-0624-x.
558 [30] H.A. Friedrichs, L.W. Ronkow, Y. Zhou, Measurement of viscosity, density and surface
559 tension of metal melts, Steel research, 68 (1997) 209-214,
560 https://doi.org/10.1002/srin.199701780.
561 [31] A. Pamies, C.G. Cordovilla, E. Louis, The measurement of surface tension of liquid
562 aluminium by means of the maximum bubble pressure method: the effect of surface oxidation,
563 Scripta metallurgica, 18 (1984) 869-872, https://doi.org/10.1016/0036-9748(84)90251-5.
564 [32] D. Wheeler, J.A. Warren, W.J. Boettinger, Modeling the early stages of reactive wetting,
565 Physical Review E, 82 (2010) 051601, https://doi.org/10.1103/PhysRevE.82.051601.
566 [33] T. Lim, S. Han, J. Chung, J.T. Chung, S. Ko, C.P. Grigoropoulos, Experimental study on
567 spreading and evaporation of inkjet printed pico-liter droplet on a heated substrate,
568 International Journal of Heat and Mass Transfer, 52 (2009) 431-441,
569 https://doi.org/10.1016/j.ijheatmasstransfer.2008.05.028.
570 [34] M.J. Assael, K. Kakosimos, R.M. Banish, J. Brillo, I. Egry, R. Brooks, P.N. Quested, K.C.
571 Mills, A. Nagashima, Y. Sato, Reference data for the density and viscosity of liquid aluminum
572 and liquid iron, Journal of physical and chemical reference data, 35 (2006) 285-300,
573 https://doi.org/10.1063/1.2149380.
574 [35] S. Schiaffino, A.A. Sonin, Molten droplet deposition and solidification at low Weber
575 numbers, Physics of fluids, 9 (1997) 3172-3187, https://doi.org/10.1063/1.869434.
576 [36] S. Rosenblat, S. Davis, How do liquid drops spread on solids?, in: Frontiers in fluid
577 mechanics, Springer, 1985, pp. 171-183, https://doi.org/10.1007/978-3-642-46543-7_9.
578 [37] B. Khina, B. Formanek, Modeling heterogeneous interaction during SHS in the Ni-Al
579 system: a phase-formation-mechanism map, International Journal of Self-Propagating High-
580 Temperature Synthesis, 16 (2007) 51-61, https://doi.org/10.3103/S106138620702001X.

[38] Q. Lin, F. Li, P. Jin, W. Zhong, Wetting of T2 Cu by molten 4043 and 6061 Al alloys at 923–1023 K, Journal of Alloys and Compounds, 734 (2018) 144-151.
[39] D. Giuranno, A. Tuissi, R. Novakovic, E. Ricci, Surface tension and density of Al− Ni Alloys, Journal of Chemical & Engineering Data, 55 (2010) 3024-3028, https://doi.org/10.1021/je901055j.
[40] I. Egry, J. Brillo, D. Holland-Moritz, Y. Plevachuk, The surface tension of liquid aluminium-based alloys, Materials Science and Engineering: A, 495 (2008) 14-18, https://doi.org/10.1016/j.msea.2007.07.104.
[41] R.K. Wunderlich, H.-J. Fecht, Surface tension and viscosity of NiAl catalytic precursor alloys from microgravity experiments, International journal of materials research, 102 (2011) 1164-1173, https://doi.org/10.3139/146.110572.
[42] R.K. Wunderlich, H.-J. Fecht, G. Lohöfer, Surface tension and viscosity of the Ni-based superalloys LEK94 and CMSX-10 measured by the oscillating drop method on board a parabolic flight, Metallurgical and Materials Transactions B, 48 (2017) 237-246, https://doi.org/10.1007/s11663-016-0847-y.
[43] R. Novakovic, M. Mohr, D. Giuranno, E. Ricci, J. Brillo, R. Wunderlich, I. Egry, Y. Plevachuk, H.J. Fecht, Surface Properties of Liquid Al-Ni Alloys: Experiments Vs Theory, Microgravity Science and Technology, 32 (2020) 1049-1064, https://doi.org/10.1007/s12217-020-09832-w.
[44] G. López, S. Sommadossi, P. Zieba, W. Gust, E. Mittemeijer, Kinetic behaviour of diffusion-soldered Ni/Al/Ni interconnections, Materials chemistry and physics, 78 (2003) 459-463, https://doi.org/10.1016/S0254-0584(02)00232-8.
[45] Z. Ding, Q. Hu, W. Lu, S. Sun, M. Xia, J. Li, In situ observation on the formation of intermetallics compounds at the interface of liquid Al/solid Ni, Scripta Materialia, 130 (2017) 214-218, https://doi.org/10.1016/j.scriptamat.2016.12.010.
[46] K. Bouche, F. Barbier, A. Coulet, Phase formation during dissolution of nickel in liquid aluminium, Zeitschrift für Metallkunde, 88 (1997) 446-451.
[47] J. Zhao, C. Unuvar, U. Anselmi-Tamburini, Z. Munir, Kinetics of current-enhanced dissolution of nickel in liquid aluminum, Acta materialia, 55 (2007) 5592-5600, https://doi.org/10.1016/j.actamat.2007.06.016.
[48] X. Ren, G. Chen, W. Zhou, C. Wu, J. Zhang, Formation and growth kinetics of intermediate phases in Ni-Al diffusion couples, Journal of Wuhan University of Technology-Mater. Sci. Ed., 24 (2009) 787, https://doi.org/10.1007/s11595-009-5787-9.
[49] G. Yu, H. Wang, S. Chen, L. Wei, J. Huang, J. Yang, Z. Zhao, Interfacial reaction between solid Ni and liquid Al in tens of seconds: Dissolution kinetics of solid Ni and formation of intermetallic compounds, Materials Characterization, 159 (2020) 110043, https://doi.org/10.1016/j.matchar.2019.110043.
[50] H. Mehrer, Diffusion in intermetallics, Materials Transactions, JIM, 37 (1996) 1259-1280, https://doi.org/10.2320/matertrans1989.37.1259.
[51] M. Adabi, A.A. Amadeh, Formation mechanisms of Ni–Al intermetallics during heat treatment of Ni coating on 6061 Al substrate, Transactions of Nonferrous Metals Society of China, 25 (2015) 3959-3966, https://doi.org/10.1016/S1003-6326(15)64073-0.
[52] S. Jung, Y. Minamino, T. Yamane, S. Saji, Reaction diffusion and formation of Al 3 Ni and Al 3 Ni 2 phases in the Al-Ni system, Journal of materials science letters, 12 (1993) 1684-1686,

https://doi.org/10.1007/BF00418831.
[53] M. Hasegawa, Ellingham diagram, in: Treatise on Process Metallurgy, Elsevier, 2014, pp. 507-516, https://doi.org/10.1016/B978-0-08-096986-2.00032-1.
[54] P. Protsenko, A. Terlain, V. Traskine, N. Eustathopoulos, The role of intermetallics in wetting in metallic systems, Scripta Materialia, 45 (2001) 1439-1445, https://doi.org/10.1016/S1359-6462(01)01181-2.
[55] K. Landry, C. Rado, R. Voitovich, N. Eustathopoulos, Mechanisms of reactive wetting: the question of triple line configuration, Acta materialia, 45 (1997) 3079-3085, https://doi.org/10.1016/S1359-6454(96)00372-2.
[56] N. Eustathopoulos, M.G. Nicholas, B. Drevet, Wettability at high temperatures, Elsevier, 1999.
[57] X.A. Zhao, H.Y. Yang, E. Ma, M.A. Nicolet, Kinetics of NiAl3 growth induced by steady‐state thermal annealing at the Ni‐interface, Journal of applied physics, 62 (1987) 1821-1825, https://doi.org/10.1063/1.339563.
[58] J.C. Liu, J. Mayer, J. Barbour, Phase formation of NiAl3 on lateral diffusion couples, Journal of applied physics, 64 (1988) 651-655, https://doi.org/10.1063/1.341956..
[59] D. Seveno, T.D. Blake, J. De Coninck, Young's equation at the nanoscale, Physical review letters, 111 (2013) 096101, https://doi.org/10.1103/PhysRevLett.111.096101.